

Probing Crust Meltdown in Inspiraling Binary Neutron Stars

Zhen Pan,¹ Zhenwei Lyu,^{1,2} Béatrice Bonga,^{3,1} Néstor Ortiz,⁴ and Huan Yang^{1,2}

¹*Perimeter Institute for Theoretical Physics, Waterloo, Ontario N2L 2Y5, Canada*

²*University of Guelph, Guelph, Ontario N2L 3G1, Canada*

³*Institute for Mathematics, Astrophysics and Particle Physics,
Radboud University, 6525 AJ Nijmegen, The Netherlands*

⁴*Instituto de Ciencias Nucleares, Universidad Nacional Autónoma de México,
Circuito Exterior C.U., A.P. 70-543, México D.F. 04510, México*

Thanks to recent measurements of tidal deformability and radius, the nuclear equation of state and structure of neutron stars are now better understood. Here, we show that through resonant tidal excitations in a binary inspiral, the neutron crust generically undergoes elastic-to-plastic transition, which leads to crust heating and eventually meltdown. This process could induce $\sim \mathcal{O}(0.1)$ phase shift in the gravitational waveform. Detecting the timing and induced phase shift of this crust meltdown will shed light on the crust structure, such as the core-crust transition density, which previous measurements are insensitive to. A direct search using GW170817 data has not found this signal, possibly due to limited signal-to-noise ratio. We predict that such signal may be observable with Advanced LIGO Plus and more likely with third-generation gravitational-wave detectors such as the Einstein Telescope and Cosmic Explorer.

Inspiraling neutron stars deform under mutual tidal interactions. In the adiabatic limit, the star's induced quadrupole moment is directly proportional to the tidal gravitational field, with the proportionality constant given by the tidal Love number. Deformed neutron stars orbit each other differently from black holes with the same masses, and the phase difference can be used to measure the tidal Love number [1], as shown in the analysis of GW170817 [2]. Together with neutron star radius measurements [3], maximum mass estimates [4] and possibly post-merger electromagnetic signals [5], the star's equation of state (EoS) is now better constrained.

In addition to adiabatic tides, tidal interaction can excite internal modes of neutron stars as the binary sweeps through the inspiral frequency range. The pressure (p-) and fundamental (f-)modes [6] will not be fully excited as their frequencies are generally higher than the inspiral frequency, although it has been suggested that early excitation of f-modes may be observed in the late inspiral stage [7]. Gravity modes may be fully excited, but their couplings to tidal gravitational fields are so small that the induced phase shifts are $\mathcal{O}(10^{-3})$ or smaller [8, 9]. Resonance of rotational modes has also been investigated assuming a rotational frequency of a few $\times 10^2$ Hz [10–12], whereas the fastest rotating pulsar known in a binary neutron star system has a frequency of ~ 44 Hz [13].

The interface (i-)modes [14], excited at the interface of the fluid core and solid crust, have frequencies around several tens to a few hundred Hertz, depending on the star's equation of state and prescription of the crust. The resonance of i-modes was proposed to explain precursors of short gamma-ray bursts due to possible crust failures [15]. We observe that through excitation of i-modes, the crustal material actually reaches its elastic limit well before the mode resonance. After reaching this threshold the crust undergoes an elastic-to-plastic transition and

the tidal driving starts to heat up the crust. The whole process ends with the meltdown of the crust in tens of cycles.

Results

Crust heating up and melting down. The outer part of the crust is commonly described by a Coulomb lattice with shear modulus μ [16]. The inner crust may have nonuniform structures associated with the “nuclear pasta” phase [17, 18], which is not considered in this study. Simulations of molecular dynamics [19] have shown that the lattice responds elastically under small applied stress; once the induced strain exceeds the breaking strain ($\epsilon_b \sim 0.1$), plastic motion starts to develop. Assuming an applied stress σ , the plastic creep rate is well approximated by [19]

$$\dot{\epsilon}_{\text{pl}} = \frac{n_i Z^2 e^2}{a} \frac{\omega_p}{\mu \bar{N} \Gamma} e^{(-18.5 \bar{\sigma}_b + \bar{\sigma} \bar{N}) \Gamma}, \quad (1)$$

where the dot denotes a time derivative, ω_p is the plasma frequency, $\bar{N} = 500/(\Gamma - 149) + 18.5$, $\bar{\sigma} = \sigma/(n_i Z^2 e^2/a)$ and $\Gamma = Z^2 e^2/aT$ is the melting parameter with e the electron charge, Ze the total charge per ion, a the lattice spacing, n_i the ion density and T the temperature. The elastic part of the strain ϵ_{el} satisfies $\sigma = \mu \epsilon_{\text{el}}$ and the total strain is simply $\epsilon = \epsilon_{\text{el}} + \epsilon_{\text{pl}}$.

With the plastic deformation, mode energy dissipates into thermal energy, which heats up the crust at a rate [20]

$$n_i \dot{e}_i = \sigma \dot{\epsilon}_{\text{pl}}(\sigma, T), \quad (2)$$

where e_i is the thermal energy per ion, and $de_i = cvdT$ with c_v the specific heat capacity for $T < T_{\text{melt}}$ [21]. Once the melting temperature T_{melt} is reached, the crustal material still needs an extra amount of latent heat ($\sim kT_{\text{melt}}$ per ion) to be melted [22]. As a result, the

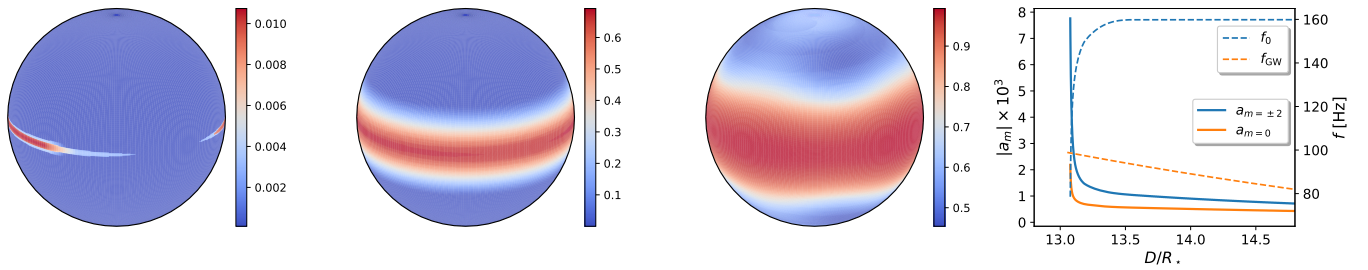


FIG. 1. Left three panels are the heat maps e_i/e_{melt} of the neutron star crust (within a $1.3M_{\odot} + 1.3M_{\odot}$ binary) at binary separations $D = 13.56/13.21/13.08 R_{\star}$, respectively. In the rightmost panel, dashed lines denote the evolution of the i-mode frequency f_0 and the GW frequency f_{GW} , and solid lines denote the evolution of mode amplitude a_m with $m = \pm 2, 0$.

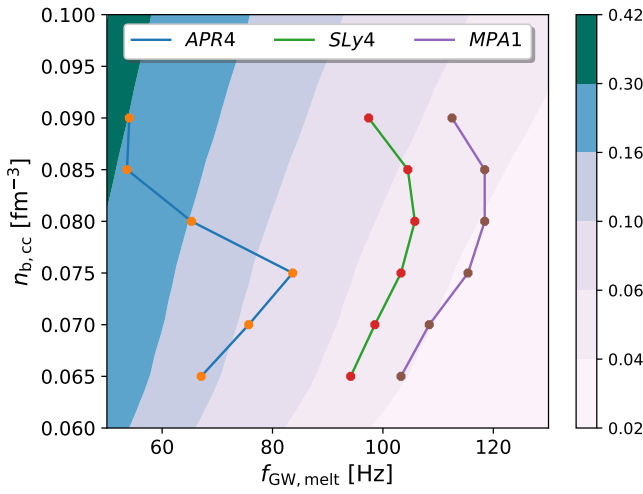


FIG. 2. The crust melting induced phase change $\delta\phi_a$ in GWs of a BNS merger with each star of $M_{\star} = 1.3M_{\odot}$ and $R_{\star} = 11.3/11.7/12.7$ km for the EoS APR4/SLy4/MPA1, respectively, which are not ruled out by the LIGO tidal measurement with GW170817.

total energy per ion needed to melt the crust from its initial cold state is roughly $e_{\text{melt}} = \int_0^{T_{\text{melt}}} c_V dT + kT_{\text{melt}}$. In this work we have ignored contributions from dripped neutrons as their specific heat may be suppressed by superfluidity.

As the neutron star binary spirals inward, the tidal field increases and so does the i-mode amplitude $a_{m=0,\pm 2}$ (m being the azimuthal wave number), as shown in Fig. 1 assuming SLy4 EoS [23, 24]. At a certain binary separation (with corresponding gravitational wave frequency $f_{\text{GW,melt}} < f_0$), part of the crust reaches the yield limit ϵ_b due to the i-mode excitation and plastic creeping starts. Heating first takes place at the equator where the strain maximizes. As the crust heats up, it softens so that i-mode frequency f_0 decreases and the mode amplitude a_m increases. As a result, the crust yields on larger and larger areas, extending from the equator to the poles, and finally the whole crust is melted. The crust melting

takes about 20 orbit periods and a total amount of energy $E_{\text{melt}} \simeq 1.1 \times 10^{47}$ ergs. Notice that this mode treatment is approximate once the plastic motion turns on, where a more accurate description requires 3-dimensional dynamical modeling of crustal motions. A 2-dimensional consistent evolution was implemented in [20] to reveal yield patterns of magnetar crust under strong magnetic stress.

Waveform signature. After the melting process, part of the binary orbital energy is converted to the mode and thermal energy resulting in a phase shift of the gravitational waveform. Similar to the discussion in [8, 9] for mode resonances, for the binary neutron star waveform $h(f) = A(f)e^{i\Psi(f)}$, its phase is modified as

$$\begin{aligned} \delta\Psi(f) &= \sum_{i=1,2} \delta\phi_i \left(1 - \frac{f}{f_i} \right) \Theta(f - f_i) \\ &\approx \delta\phi_a \left(1 - \frac{f}{f_a} \right) \Theta(f - f_a) \end{aligned} \quad (3)$$

where Θ is the Heaviside function and f_i is the melting frequency of each star. Therefore the search and forecast presented below for crust melting applies equally for generic mode resonances, so that we will not distinguish these terms. The melting process increases the coalescence phase by $\delta\phi_i$ and the coalescence time by $\delta\phi_i/f_i$. In the second line we introduced $\delta\phi_a = \sum_i \delta\phi_i$ and $\delta\phi_a/f_a = \sum_i \delta\phi_i/f_i$ to reduce the number of extra parameters in this model, which simplifies the parameter estimation process. Notice that if energy transfers from the orbit to the mode (or heat in this case) during resonance, $\delta\phi$ is positive; if energy transfers from the mode to the orbit, as expected in some of the r-mode resonances [12], $\delta\phi$ is negative.

For each neutron star, $\delta\phi$ depends on its mass M_{\star} , the mass ratio of the companion q , the melting energy E_{melt} and the melting frequency $f_{\text{GW,melt}}$ as follows [8]

$$\delta\phi = \frac{2\omega_{\text{orb}}E_{\text{melt}}}{P_{\text{GW}}} \simeq \frac{0.1}{q^2} \left(\frac{1+q}{2} \right)^{2/3} E_{47} M_{1.3}^{-10/3} f_{70}^{-7/3}, \quad (4)$$

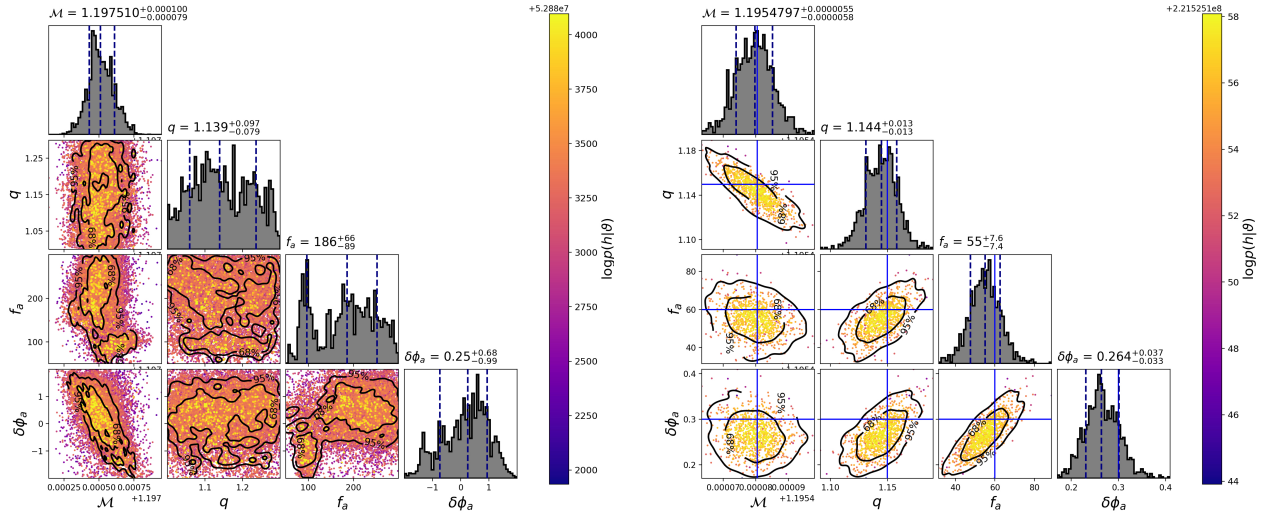


FIG. 3. Posterior distribution of chirp mass \mathcal{M} , mass ratio q , phase shift $\delta\phi_a$ and melting frequency f_a obtained with PyCBC. Left Plot: the search uses data from GW170817, where the prior for f_a is set to be $[50, 200]$ Hz and $[-2, 2]$ for $\delta\phi_a$. Right Plot: a search obtained assuming LIGO A+ sensitivity and an injection at $f_a = 60$ Hz and $\delta\phi_a = 0.3$. The priors of f_a and $\delta\phi_a$ are set to be $[31, 200]$ Hz and $[-1, 1]$.

where $\omega_{\text{orb}} = \pi f_{\text{GW,melt}}$ is the orbital angular frequency, P_{GW} is the energy loss rate due to GW emission, and $E_{47} = E_{\text{melt}}/10^{47}$ ergs, $M_{1.3} = M_{\star}/1.3M_{\odot}$, $f_{70} = f_{\text{GW,melt}}/70$ Hz. We immediately see that the phase shift increases if the melting process happens earlier in the inspiral phase. In Fig. 2, we show the total phase change $\delta\phi_a$ for an equal-mass BNS merger with $M_{\star} = 1.3M_{\odot}$, where $\delta\phi_a$ varies from 0.04 to 0.3 depending on the star’s EoS and the core-crust transition baryon density $n_{\text{b,cc}}$. The melting energy increases substantially with increasing $n_{\text{b,cc}}$ (commonly assumed to be within $0.06 - 0.1$ fm $^{-3}$ [25–27]), whereas the i-mode frequency and the associated melting frequency are non-monotonic functions of $n_{\text{b,cc}}$. We also note that since the mode calculation presented here is Newtonian with the Cowling approximation [28], the fully relativistic mode frequencies may be different (for examples, the frequencies of p- and f-modes are smaller with the metric perturbation included [29, 30]). If there are also more unpaired neutrons present within the star, as suggested by the cooling measurement in [31], the melting energy may be significantly boosted and the internal mode spectrum may be modified as well. The effects of nuclear pastas on the melting energy budget and the mode frequency determination also need to be better understood. Nevertheless, the measurement of $f_{\text{GW,melt}}$ and $\delta\phi_a$ will convey useful information about the core-crust transition density and the star’s EoS around that density.

Search with GW170817. We now present the first search for mode resonance effects (including crust melt-

ing) in binary neutron star systems with data from GW170817 with Equation (3) implemented. A similar search for tidal-p-g instability is discussed in [32] using different $\delta\Psi(f)$. The Markov-Chain Monte Carlo parameter estimation is performed with PyCBC [33], for which we assume the source distance and sky location are known as the electromagnetic counterpart of this source has been identified [34]. We use the TaylorF2 waveform [35] as the background binary neutron waveform. We present the posterior distributions of chirp mass, mass ratio, $\delta\phi_a$ and f_a in Fig. 3. The marginal distribution of $\delta\phi_a$ indicates that there is no evidence for mode resonance in GW170817, as the uncertainty in $\delta\phi_a$ is roughly $0.7 - 1.0$. A similar conclusion can be drawn from a Bayesian model comparison framework. We denote \mathcal{H}_a as the hypothesis with mode resonance and \mathcal{H}_0 as the one without, the Bayes factor can be defined as

$$\mathcal{B}_0^a = \frac{P(\text{GW170817}|\mathcal{H}_a)}{P(\text{GW170817}|\mathcal{H}_0)} \quad (5)$$

which measures the relative probability of these two hypotheses. We have computed the Bayes factor using both the method of thermodynamic integration [36] and the Savage-Dickey Density Ratio method [37], which both suggest consistent values of $\log \mathcal{B}_0^a$ in the range of $[-0.5, -0.3]$. This means that these two hypotheses are essentially indistinguishable with this set of gravitational wave data [38].

It is natural to expect observations with higher signal-to-noise ratios as the sensitivity of gravitational wave detectors improves. In the mid-2020s the upgrade of Ad-

vanced LIGO, LIGO A+, is expected to be built [39]. Assuming LIGO A+ design sensitivity for both detectors at Hanford and Livingston, and Advanced Virgo with its full sensitivity, we may observe GW170817-like events with signal-to-noise ratios beyond 100. In the right panel of Fig. 3, we present a sample search with an injected signal with $\delta\phi_a = 0.3$, $f_a = 60\text{Hz}$ (for a GW170817-type system) into simulated detector noises consistent with the aforementioned LIGO A+ network sensitivity. The measurement uncertainty in $\delta\phi_a$ is $\sim 0.04 - 0.2$ depending on f_a . So it is possible that we observe the effect of crust melting in gravitational waves with LIGO A+. Stacking different events may also improve detectability, as is the case for subdominant modes in black hole ring-downs [40]. However, we have no prior information on $\delta\phi_a$ and f_a , which are distinct for each binary neutron star system.

If a mode resonance signature is indeed detected (i.e. preferred over the null hypothesis), it is still necessary to compare to other possible origins, such as tidal-p-g coupling [32] and dynamical scalarization [41, 42], and scalar modes associated to certain GR extensions [43], that predict different $\delta\Psi(f)$. To simulate this, we inject a mode resonance signal ($\delta\phi_a = 0.3$, $f_a = 60\text{Hz}$) into detector noise corresponding to the LIGO A+ network, and perform the Bayesian model selection between our model resonance waveform and the tidal-p-g waveform. The Bayes factor is $\log \mathcal{B}_{p-g}^a \sim 6.1 \pm 2.4$, suggesting that it is also possible to determine the correct model if a positive detection occurs. The comparison is much sharper with third-generation gravitational wave detectors.

Discussion

Resonant tidal excitations in a neutron star binary induce a phase shift $\delta\phi_a$ in the gravitational wave signal by melting its crust. LIGO A+ may already be able to detect such induced phase shifts. A 3rd-generation detector network with Cosmic Explorer [44] sensitivity at the LIGO detectors and Einstein Telescope [45] sensitivity at the Virgo detector is able to limit $\delta\phi_a$ with uncertainty ~ 0.01 and f_a below 1%. This will not only allow high-confidence detection of the crust melting effect, but also precisely measure crustal and EoS properties as shown in Fig. 2.

We do not expect significant energy release to the neutron star magnetosphere associated with crustal failure, as the magnetic fields ($\sim 10^{12}\text{G}$) assumed are too weak to efficiently transfer energy by sending out Alfvén waves. However, if the star is a magnetar with field $\sim 10^{15}$ G, this emission mechanism may excite star magnetospheres and power precursor gamma-ray bursts [20, 46, 47]. Interestingly, the recent LIGO observation of a heavy neutron-star binary (GW190425 [48]) may indicate the existence of a fast-merging channel to form binary neutron stars. Such systems may have short-enough lifetime $\sim 10^4$ years to allow active magnetars in the bi-

nary coalescence stage [49].

Methods

I-mode calculation. In the linear approximation, the stellar response to the tidal force is specified by the Lagrangian displacement $\xi(\mathbf{r}, t)$ of a fluid element from its equilibrium position. The displacement can be decomposed into eigenmodes, $\xi(\mathbf{r}, t) = \sum_\alpha a_\alpha(t) \xi_\alpha(\mathbf{r})$, where α denotes the quantum number of an eigenmode. In the context of this paper, we only consider spheroidal modes driven by the leading quadrupole term of the tidal force, so that $\xi_m(\mathbf{r}) = [U(r)\hat{r} + rV(r)\nabla]Y_{2m}(\theta, \phi)$. Its behavior is governed by the following linear equation [14]

$$\omega_0^2 \begin{bmatrix} U \\ V \end{bmatrix} = \mathcal{L}(r; \mu) \begin{bmatrix} U \\ V \end{bmatrix}, \quad (6)$$

where $Y_{2m}(\theta, \phi)$ is the $l = 2$ spherical harmonic and ω_0 the eigenfrequency. We applied the Cowling approximation by assuming negligible perturbations of the gravitational potential [28]. On the right-hand side, \mathcal{L} is an operator specifying the internal restoring forces of the star. In general, \mathcal{L} is a second-order differential operator and degrades to be first-order in the limit of vanishing shear modulus $\mu \rightarrow 0$. In the crust, the shear modulus μ is calculated according to [16]

$$\mu = \frac{0.1194}{1 + 0.595(\Gamma_{\text{melt}}/\Gamma)^2} \frac{n_i(Ze)^2}{a}, \quad (7)$$

where $\Gamma_{\text{melt}} \simeq 176$ is the value of the melting parameter $\Gamma(T = T_{\text{melt}})$ at melting temperature [50].

To solve the above eigenvalue problem, we specify three boundary conditions by the regularity condition at $r \rightarrow 0$ and vanishing radial and transverse tractions at $r \rightarrow R_\star$. The continuity conditions at the core-crust interface can be matched using a standard shooting routine. For the example star used in the main text, we obtain an i-mode eigenfrequency $f_0 = \omega_0/2\pi = 160$ Hz. The eigenfunctions $U(r)$ and $V(r)$ determine the tidal coupling coefficient through [15]

$$Q = \frac{1}{M_\star R_\star^2} \int d^3x \rho \xi_m^* \cdot \nabla[r^2 Y_{2m}(\theta, \phi)] = 0.017, \quad (8)$$

with the normalization $\langle \xi_m | \xi_m \rangle := \int d^3x \rho \xi_m \cdot \xi_m^* = \delta_{mm'} M_\star R_\star^2$, where ρ is the mass density.

Crust melting. The evolution of the mode amplitude $a_m(t)$ is governed by [8]

$$\ddot{a}_m + \gamma(t)\dot{a}_m + \omega_0^2(t)a_m = \frac{GM'W_{2m}Q}{D^3}e^{-im\Phi(t)}, \quad (9)$$

where the right-hand side is the leading quadrupole term of the tidal driving force with G the gravitational constant, $M' = qM_\star$ the companion star mass, D the binary

seperation, W_{2m} a numerical coefficient of $\mathcal{O}(1)$ and $\Phi(t)$ the orbital phase. On the left-hand side, $\gamma(t)$ is the friction coefficient capturing the plastic deformation induced dissipation

$$\gamma(t) = \frac{N_i \langle \dot{e}_i \rangle}{M_\star R_\star^2 \sum_m |\dot{a}_m|^2}, \quad (10)$$

with N_i the total number of ions in the crust and $\langle \dot{e}_i \rangle$ the average heating rate per ion. The eigenfrequency $\omega_0(t)$ to leading order is determined by

$$\omega_0^2(t) = \frac{\langle \xi_m | \mathcal{L}(r; \mu_{\text{avg}}) \xi_m \rangle}{\langle \xi_m | \xi_m \rangle}, \quad (11)$$

where μ_{avg} is the average shear modulus which decreases as the crust is heated.

Given the mode amplitude $a_m(t)$, it is straightforward to calculate the fluid element displacement $\xi(\mathbf{r}, t) = \sum_m a_m(t) \xi_m(\mathbf{r})$ and the corresponding strain ϵ_{el} . From equation (1), the plastic deform rate $\dot{\epsilon}_{\text{pl}}$ has an exponential dependence on the local strain ϵ_{el} for $\epsilon_{\text{el}} \gtrsim 0.1$, so does the energy dissipation rate $\sigma \dot{\epsilon}_{\text{pl}}$. Physically, the dissipated energy comes from the local elastic energy, therefore the energy dissipation rate cannot exceed its replenishment rate $\frac{\mathcal{A}}{2} \mu \epsilon_{\text{el}}^2 f_{\text{GW}}$, where f_{GW} is the frequency of both the tidal force and the GWs and \mathcal{A} is a coefficient of $\mathcal{O}(1)$. In the main text, we choose $\mathcal{A} = 2$ as an example. As for the initial condition, we choose $T_i = 0.02T_{\text{melt}}$, where T_{melt} is the melting temperature of the ion crystal at the crust base. Using the 4th-order Runge-Kutta scheme, we evolve equations (1, 2, 9) on the two-dimensional surface of the crust base, i.e., we only trace the thermal evolution of the crust base considering its dominant role in the crust heat capacity.

Bayesian parameter estimation and model test. For the search of possible mode resonance in GW170817, we have incorporated $\delta\phi_a, f_a$ plus all the binary parameters (except for the source distance and sky location which are known from electromagnetic counterparts), including chirp mass \mathcal{M} , mass ratio q , inclination angle ι , polarization phase ψ_c , coalescence phase ϕ_c , coalescence time t_c , tidal Love numbers of both stars $\Lambda_{1,2}$ and parallel spins of both stars $\chi_{1,2z}$. The priors of the spin are set to be $|\chi_{1,2z}| < 0.05$. The full posterior distribution of parameters and the Markov-Chain Monte-Carlo samples are presented in Fig. 4. In general, the accuracy of the search result not only depends on the event signal-to-noise ratio, but also on the melting frequency. If the melting frequency is too small, even if it is still in the LIGO band, the imbalance of the waveform signal-to-noise ratio before and after the melting process still degrades the search accuracy. For GW170817, given that the low-frequency sensitivity of the LIGO detectors in O2 is significantly worse than O3, we find that it is beneficial to set the lower bound of the frequency range to be

at least 40 Hz to allow SNR ~ 5 in the waveform before the resonance. This situation will be greatly improved as LIGO reaches design sensitivity when the low-frequency performance is much better, and definitely for LIGO A+ and 3rd-generation detectors, which is important as crust melting may happen before 40 Hz.

To compare two models or hypotheses, we apply the Bayesian model selection method. For hypothesis \mathcal{H}_1 and \mathcal{H}_0 and observed data s , the Bayes factor is defined as

$$\mathcal{B}_0^1 = \frac{P(s|\mathcal{H}_1)}{P(s|\mathcal{H}_0)}. \quad (12)$$

The probability functions $P(s|\mathcal{H}_{0,1})$ are usually referred to as the evidence, which may be computed with various tools, such as the thermodynamic integration method [36] and the Savage-Dickey Density Ratio method [37]. Larger Bayes factor \mathcal{B}_0^1 implies more preference of hypothesis 1 over hypothesis 0, and vice versa. According to the justification in [38], if $-1.1 < \log \mathcal{B}_0^1 < 1.1$, the data does not prefer one model over the other; if $1.1 < \log \mathcal{B}_0^1 < 3$, there is positive support for model 1; if $3 < \log \mathcal{B}_0^1 < 5$, there is strong support for model 1 and if $\log \mathcal{B}_0^1 > 5$, the support is overwhelming. We have applied such formalism in the search for a resonance signature in the data of GW170817, in which case \mathcal{H}_1 is the model including the resonance effect and the null hypothesis \mathcal{H}_0 is the one without. We obtain $\log \mathcal{B}_0^1 \sim [-0.5, -0.3]$, so that there is no evidence of mode resonance in the parameter range we searched for in the strain data of GW170817.

The model selection method also applies to distinguish possible origins of the signal. For example, if we detect a signal by searching with our mode resonance waveform, it may also show a positive signal if we had searched for this signal with waveforms motivated by other reasons. To illustrate this, we injected a mode resonance signal ($\delta\phi_a = 0.3, f_a = 60\text{Hz}$) to simulated detector noise compatible with LIGO A+, and searched it with both our mode resonance waveform (Eq. 3) and the waveform for tidal-p-g coupling [32]:

$$\delta\Psi(f) = -\frac{2C}{3B^2(3-n_0)(4-n_0)} \left\{ \Theta\left(\frac{f}{f_{\text{ref}}}\right)^{n_0-3} (1-\Theta)\left(\frac{f}{f_{\text{ref}}}\right)^{n_0-3} \left[(4-n_0) - (3-n_0)\left(\frac{f}{f_{\text{ref}}}\right) \right] \right\}, \quad (13)$$

where $\Theta = \Theta(f - f_0)$, $f_{\text{ref}} = 100\text{Hz}$, $C = A_0(m_1^{2/3} + m_2^{2/3})/M^{2/3}$, and $B = (32/5)(G\mathcal{M}\pi f_{\text{ref}}/c^3)^{5/3}$. The corresponding posterior distributions of parameters are shown in Fig. 5. The fitting with tidal-p-g coupling does not generate a compact posterior distribution of the parameters of this odel, A_0, f_0 and n_0 , although the distribution of $\log A_0$ is significantly different from the lower bound of its prior, which is -10. As we compare the

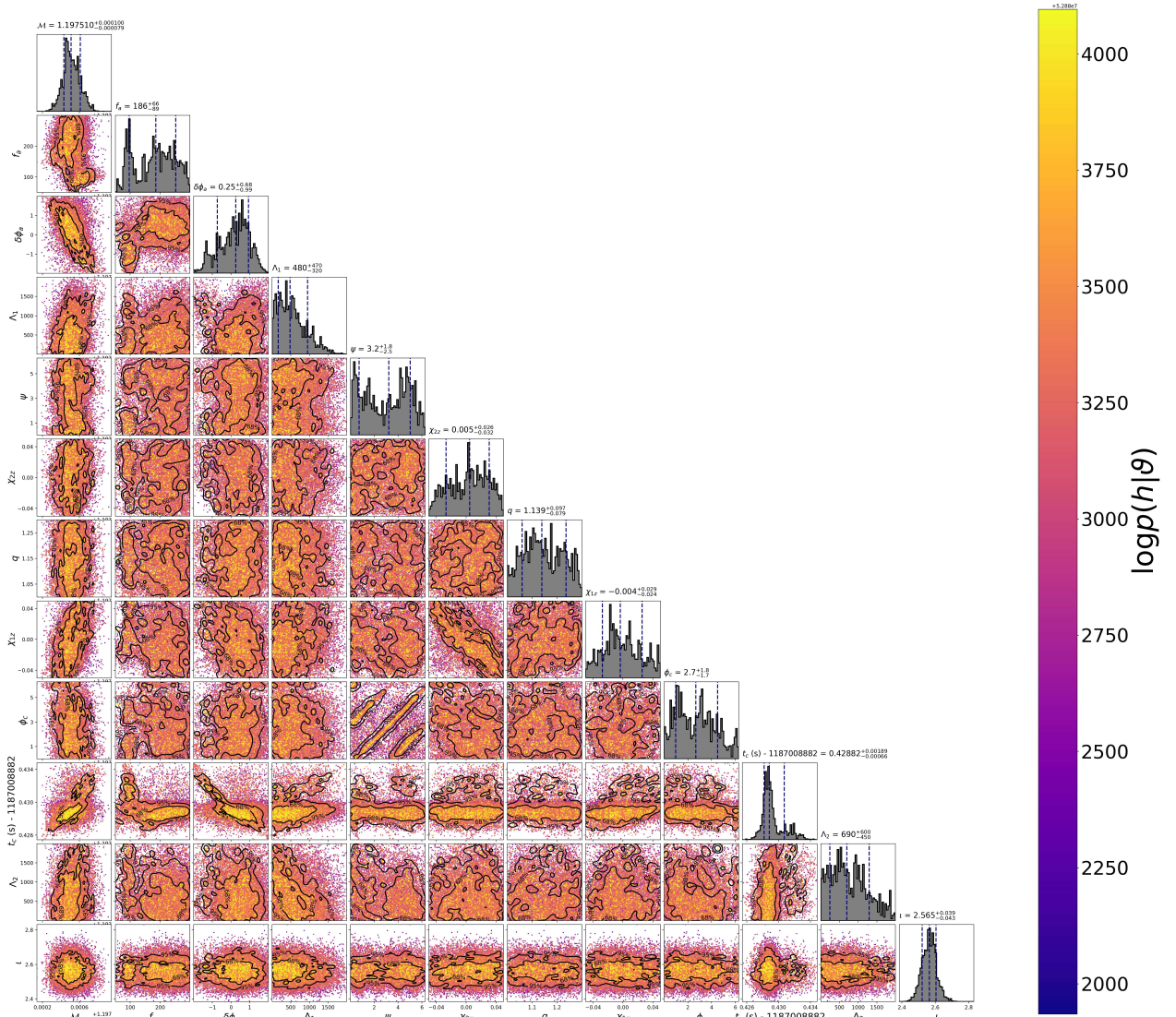


FIG. 4. The posterior distribution of all parameters in the search of mode resonance presented in Fig. 3 with data from GW170817.

two models, the Bayes factor $\log \mathcal{B}_{\text{pg}}^{\text{res}}$ is 6.1 ± 2.4 , which shows clear preference for the mode resonance model. This means that it is still possible to distinguish these two models when we detect a mode resonance signal with LIGO A+.

Acknowledgement. We thank David Tsang for sharing the code for neutron star mode analysis. Z. P., Z. L. and H. Y. are supported by the Natural Sciences and

Engineering Research Council of Canada and in part by Perimeter Institute for Theoretical Physics. Research at Perimeter Institute is supported in part by the Government of Canada through the Department of Innovation, Science and Economic Development Canada and by the Province of Ontario through the Ministry of Colleges and Universities.

Author Contributions. Z.P. performed the mode analysis, calculated the crust melting and the induced

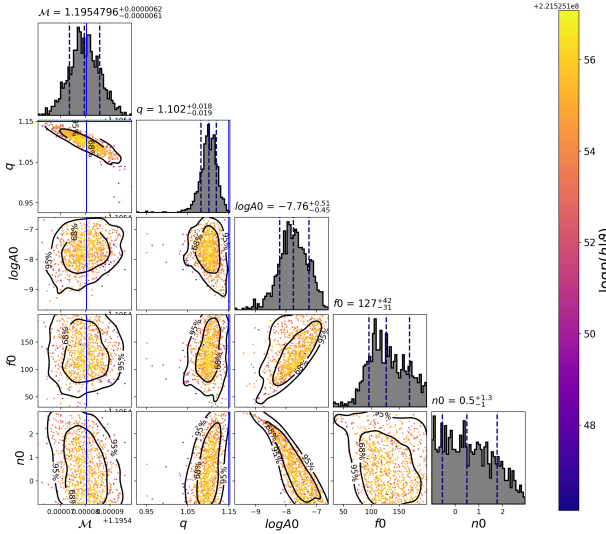


FIG. 5. The posterior distribution of chirp mass, mass ratio and A_0, n_0, f_0 as we try to fit the waveform discussed in Fig. 3 with the tidal-p-g mode waveform.

phase shift in the gravitational waves. Z.L. did the mode resonance search in GW170817 and the forecast for future detectors. B.B. derived the equations and did the code cross-check for the mode analysis. N.O. contributed to the mode analysis code. H.Y. developed the idea and supervised the whole project. All the authors contributed to the final manuscript.

Competing Interests. We declare no competing interests.

Correspondence. Correspondence and requests for materials should be addressed to Z.P. and H.Y. (email: zpan@perimeterinstitute.ca, hyang@perimeterinstitute.ca)

- [1] E. E. Flanagan and T. Hinderer, *Phys. Rev. D* **77**, 021502 (2008), arXiv:0709.1915 [astro-ph].
- [2] B. P. Abbott *et al.* (LIGO Scientific, Virgo), *Phys. Rev. Lett.* **121**, 161101 (2018), arXiv:1805.11581 [gr-qc].
- [3] M. C. Miller *et al.*, *Astrophys. J. Lett.* **887**, L24 (2019), arXiv:1912.05705 [astro-ph.HE].
- [4] L. Rezzolla, E. R. Most, and L. R. Weih, *Astrophys. J.* **852**, L25 (2018), [*Astrophys. J. Lett.* 852, L25(2018)], arXiv:1711.00314 [astro-ph.HE].
- [5] D. Radice, A. Perego, F. Zappa, and S. Bernuzzi, *Astrophys. J.* **852**, L29 (2018), arXiv:1711.03647 [astro-ph.HE].
- [6] K. D. Kokkotas and B. G. Schmidt, *Living Reviews in Relativity* **2**, 2 (1999), arXiv:gr-qc/9909058 [gr-qc].
- [7] G. Pratten, P. Schmidt, and T. Hinderer, (2019), arXiv:1905.00817 [gr-qc].
- [8] D. Lai, *MNRAS* **270**, 611 (1994), arXiv:astro-ph/9404062 [astro-ph].
- [9] H. Yu and N. N. Weinberg, *Mon. Not. Roy. Astron. Soc.* **464**, 2622 (2017), arXiv:1610.00745 [astro-ph.HE].
- [10] W. C. G. Ho and D. Lai, *Mon. Not. Roy. Astron. Soc.* **308**, 153 (1999), arXiv:astro-ph/9812116 [astro-ph].
- [11] D. Lai and Y. Wu, *Phys. Rev. D* **74**, 024007 (2006), arXiv:astro-ph/0604163 [astro-ph].
- [12] E. E. Flanagan and E. Racine, *Phys. Rev. D* **75**, 044001 (2007), arXiv:gr-qc/0601029 [gr-qc].
- [13] M. Burgay *et al.*, *Nature* **426**, 531 (2003), arXiv:astro-ph/0312071 [astro-ph].
- [14] P. N. McDermott, H. M. van Horn, and C. J. Hansen, *Astrophys. J.* **325**, 725 (1988).
- [15] D. Tsang, J. S. Read, T. Hinderer, A. L. Piro, and R. Bondarescu, *Phys. Rev. Lett.* **108**, 011102 (2012), arXiv:1110.0467 [astro-ph.HE].
- [16] T. Strohmayer, S. Ogata, H. Iyetomi, S. Ichimaru, and H. M. van Horn, *Astrophys. J.* **375**, 679 (1991).
- [17] D. G. Ravenhall, C. J. Pethick, and J. R. Wilson, *Phys. Rev. Lett.* **50**, 2066 (1983).
- [18] M.-a. Hashimoto, H. Seki, and M. Yamada, *Progress of Theoretical Physics* **71**, 320 (1984).
- [19] A. I. Chugunov and C. J. Horowitz, *MNRAS* **407**, L54 (2010), arXiv:1006.2279 [astro-ph.SR].
- [20] C. Thompson, H. Yang, and N. Ortiz, *Astrophys. J.* **841**, 54 (2017), arXiv:1608.02633 [astro-ph.HE].
- [21] G. Chabrier, *Astrophys. J.* **414**, 695 (1993).
- [22] S. L. Shapiro and S. A. Teukolsky, *Black holes, white dwarfs, and neutron stars : the physics of compact objects*, New York: Wiley (1983).
- [23] F. Douchin and P. Haensel, *Astronomy & Astrophysics* **380**, 151 (2001), arXiv:astro-ph/0111092 [astro-ph].
- [24] J. S. Read, B. D. Lackey, B. J. Owen, and J. L. Friedman, *Phys. Rev. D* **79**, 124032 (2009).
- [25] C. J. Horowitz and J. Piekarewicz, *Phys. Rev. Lett.* **86**, 5647 (2001), arXiv:astro-ph/0010227 [astro-ph].
- [26] J. Xu, L.-W. Chen, B.-A. Li, and H.-R. Ma, *Astrophys. J.* **697**, 1549 (2009), arXiv:0901.2309 [astro-ph.SR].
- [27] C. C. Moustakidis, T. Nikšić, G. A. Lalazissis, D. Vretenar, and P. Ring, *Phys. Rev. C* **81**, 065803 (2010), arXiv:1004.3882 [nucl-th].
- [28] T. G. Cowling, *MNRAS* **101**, 367 (1941).
- [29] S. Yoshida and Y. Kojima, *MNRAS* **289**, 117 (1997), arXiv:gr-qc/9705081 [gr-qc].
- [30] C. Chirenti, G. H. de Souza, and W. Kastaun, *Phys. Rev. D* **91**, 044034 (2015).
- [31] E. F. Brown, A. Cumming, F. J. Fattoyev, C. J. Horowitz, D. Page, and S. Reddy, *Phys. Rev. Lett.* **120**, 182701 (2018).
- [32] B. P. Abbott *et al.* (LIGO Scientific, Virgo), *Phys. Rev. Lett.* **122**, 061104 (2019), arXiv:1808.08676 [astro-ph.HE].
- [33] <https://pycbc.org/>.
- [34] B. P. Abbott, R. Abbott, T. Abbott, F. Acernese, K. Ackley, C. Adams, T. Adams, P. Adesso, R. Adhikari, V. Adya, *et al.*, *Physical Review Letters* **119**, 161101 (2017).
- [35] A. Buonanno, B. Iyer, E. Ochsner, Y. Pan, and B. S. Sathyaprakash, *Phys. Rev. D* **80**, 084043 (2009), arXiv:0907.0700 [gr-qc].
- [36] N. Lartillot and H. Philippe, *Systematic Biology* **55**, 195 (2006), <https://academic.oup.com/sysbio/article-pdf/55/2/195/26557316/10635150500433722.pdf>.

[37] J. M. Dickey, *The Annals of Mathematical Statistics* **42**, 204 (1971).

[38] R. E. Kass and A. E. Raftery, *Journal of the American Statistical Association* **90**, 773 (1995).

[39] <https://dcc.ligo.org/LIGO-G1601435/public>.

[40] H. Yang, K. Yagi, J. Blackman, L. Lehner, V. Paschalidis, F. Pretorius, and N. Yunes, *Phys. Rev. Lett.* **118**, 161101 (2017), arXiv:1701.05808 [gr-qc].

[41] C. Palenzuela, E. Barausse, M. Ponce, and L. Lehner, *Phys. Rev.* **D89**, 044024 (2014), arXiv:1310.4481 [gr-qc].

[42] L. Annuluri, V. Cardoso, and L. Gualtieri, *Phys. Rev.* **D99**, 044038 (2019), arXiv:1901.02461 [gr-qc].

[43] R. F. Mendes and N. Ortiz, *Physical Review Letters* **120** (2018), 10.1103/physrevlett.120.201104.

[44] B. P. Abbott, R. Abbott, T. D. Abbott, M. R. Abernathy, K. Ackley, C. Adams, P. Addesso, R. X. Adhikari, V. B. Adya, C. Affeldt, and et al., *Classical and Quantum Gravity* **34**, 044001 (2017), arXiv:1607.08697 [astro-ph.IM].

[45] M. Punturo *et al.*, *Proceedings, 14th Workshop on Gravitational wave data analysis (GWDAW-14): Rome, Italy, January 26-29, 2010*, *Class. Quant. Grav.* **27**, 194002 (2010).

[46] M. Ackermann *et al.* (Fermi GBM/LAT), *Nature* **462**, 331 (2009), arXiv:0908.1832 [astro-ph.HE].

[47] E. Troja, S. Rosswog, and N. Gehrels, *Astrophys. J.* **723**, 1711 (2010), arXiv:1009.1385 [astro-ph.HE].

[48] The LIGO Scientific Collaboration, the Virgo Collaboration, B. P. Abbott, R. Abbott, T. D. Abbott, S. Abraham, F. Acernese, K. Ackley, C. Adams, R. X. Adhikari, V. B. Adya, C. Affeldt, M. Agathos, K. Agatsuma, N. Aggarwal, O. D. Aguiar, L. Aiello, A. Ain, P. Ajith, G. Allen, A. Alcocka, M. A. Aloy, P. A. Altin, A. Amato, S. Anand, A. Ananyeva, S. B. Anderson, W. G. Anderson, S. V. Angelova, S. Antier, S. Appert, K. Arai, M. C. Araya, J. S. Areeda, M. Arène, N. Arnaud, S. M. Aronson, K. G. Arun, S. Ascenzi, G. Ashton, S. M. Aston, P. Astone, F. Aubin, P. Aufmuth, K. AultONeal, C. Austin, V. Avendano, A. Avila-Alvarez, S. Babak, P. Bacon, F. Badaracco, M. K. M. Bader, S. Bae, J. Baird, P. T. Baker, F. Baldaccini, G. Ballardin, S. W. Ballmer, A. Bals, S. Banagiri, J. C. Barayoga, C. Barbieri, S. E. Barclay, B. C. Barish, D. Barker, K. Barkett, S. Barnum, F. Barone, B. Barr, L. Barsotti, M. Barsuglia, D. Barta, J. Bartlett, I. Bartos, R. Bassiri, A. Basti, M. Bawaj, J. C. Bayley, A. C. Baylor, M. Bazzan, B. Bécsy, M. Bejger, I. Belahcene, A. S. Bell, D. Beniwal, M. G. Benjamin, B. K. Berger, G. Bergmann, S. Bernuzzi, C. P. L. Berry, D. Bersanetti, A. Bertolini, J. Betzwieser, R. Bhandare, J. Bidler, E. Biggs, I. A. Bilenko, S. A. Bilgili, G. Billingsley, R. Birney, O. Birnholtz, S. Biscans, M. Bischi, S. Biscoveanu, A. Bisht, M. Bitossi, M. A. Bizouard, J. K. Blackburn, J. Blackman, C. D. Blair, D. G. Blair, R. M. Blair, and S. e. a. Bloemen, (2020), arXiv:2001.01761 [astro-ph.HE].

[49] H. Yang and Y.-C. Zou, (2020), arXiv:2002.02553 [astro-ph.HE].

[50] G. S. Stringfellow, H. E. DeWitt, and W. L. Slattery, *Phys. Rev. A* **41**, 1105 (1990).